nature nanotechnology

REVIEW ARTICLE

PUBLISHED ONLINE: 1 APRIL 2012 | DOI: 10.1038/NNANO.2012.38

The emergence of multifrequency force microscopy

Ricardo Garcia* and Elena T. Herruzo

In atomic force microscopy a cantilever with a sharp tip attached to it is scanned over the surface of a sample, and information about the surface is extracted by measuring how the deflection of the cantilever — which is caused by interactions between the tip and the surface — varies with position. In the most common form of atomic force microscopy, dynamic force microscopy, the cantilever is made to vibrate at a specific frequency, and the deflection of the tip is measured at this frequency. But the motion of the cantilever is highly nonlinear, and in conventional dynamic force microscopy, information about the sample that is encoded in the deflection at frequencies other than the excitation frequency is irreversibly lost. Multifrequency force microscopy involves the excitation and/or detection of the deflection at two or more frequencies, and it has the potential to overcome limitations in the spatial resolution and acquisition times of conventional force microscopes. Here we review the development of five different modes of multifrequency force microscopy and examine its application in studies of proteins, the imaging of vibrating nanostructures, measurements of ion diffusion and subsurface imaging in cells.

The atomic force microscope (AFM) has been a key instrument in the development of nanoscience and nanotechnology over the past 25 years[1]. Unlike most forms of imaging, it does not rely on electrons or photons to probe a sample. Rather, in atomic force microscopy we measure the deflection of a probe (an extremely sharp tip attached to a flexible cantilever) as it is scanned across the surface of a sample. In the early days of the AFM the tip was always in mechanical contact with the surface, and the first images taken with 'contact AFM' barely hinted at the nanoscale spatial resolution of which the technique was capable[1]. Since then the AFM has undergone a number of improvements, and the introduction of optical methods to measure the deflection[2] paved the way for the manufacture of commercial AFM systems.

In dynamic AFM[3,4], which first emerged a few years after contact AFM, the probe is excited at a single frequency while being scanned across the sample. A feedback loop keeps one of the parameters of the oscillation — either the amplitude or the frequency shift — at a fixed value. The oscillation parameters depend on the separation between the tip and the surface, and therefore atomic or nanoscale changes in topography cause changes in this distance and, in turn, the oscillation parameters of the probe. By compensating for these changes, the feedback loop generates high-resolution images of the surface topography. Dynamic AFM has four advantages over contact AFM. First, it is easier to image at small forces (such as in the 1 nN range) especially in air, and this allows soft materials to be imaged. Second, lateral forces are suppressed. Third, observables such as the amplitude, the phase, the frequency or the cantilever deflection are available and can be used to extract information on the properties of a material. Finally, atomic resolution imaging of reactive surfaces in ultrahigh vacuum can be achieved through control over the mechanical contact between the tip and the surface atoms.

The reduction of the force exerted by the tip on the sample has been essential in allowing a variety of soft materials, such as DNA, proteins, cells or polymers[5–8], to be studied with relative ease. The reduction of the force has also led to atomic- and molecular-resolution images in a variety of environments[9–14]. Furthermore, dynamic AFM has provided a suitable experimental set-up to combine topography with the mapping of electrostatic[15] or magnetic[16] properties.

The impact of force microscopy also goes beyond the field of high-resolution imaging. In particular, it has led to a renaissance in mechanics, or more accurately, nanomechanics, which can be used to explain the operation and the performance of the AFM[3,17–19]. Moreover, AFM can be used to precisely measure the binding forces between individual biomolecules or the local stiffness of biomaterials (force spectroscopy)[20,21]. For example, force spectroscopy has been used to study the nanomechanical properties of cells[22], which could be relevant to analysing the progression of tumours[23]. In addition, AFM technology has led to the development of very sensitive micro- and nanomechanical devices[24,25].

Despite the success of AFM, the technique currently faces limitations in terms of spatial resolution, quantitative measurements and data acquisition times. Atomic- and molecular-resolution imaging in air, liquid or ultrahigh vacuum is arguably the most striking feature of the instrument. However, high-resolution imaging is a property that depends as much on the mechanical properties of the material under study as it does on the sensitivity and resolution of the microscope. Molecular-resolution images are either hard to obtain or, in the case of very soft materials such as those with an effective elastic modulus below 10 MPa (isolated proteins, cells, some polymers), have not been obtained yet. Similarly, it is hard to combine the exquisite force sensitivity of force spectroscopy with molecular-resolution imaging, and it is therefore challenging to obtain simultaneous high spatial resolution and material properties mapping.

The conventional AFM is a surface characterization technique, and the non-invasive imaging of buried structures (subsurface imaging) is not considered a mainstream activity. Similarly, processes, such as subsurface ion diffusion in batteries, have been beyond the realm of the AFM either because of a lack of sensitivity or because of difficulties in separating elastic from non-conservative components in the measured force.

To expand the capabilities of the AFM and to overcome its current limitations, two principles need to be considered: (1) all the information about the properties of a sample are encoded in the probe's motion; and (2) the dynamics of the cantilever are highly nonlinear, and therefore the harmonics and lower eigenmodes components are integral parts of the tip's motion. Conventional dynamic AFM methods involve the excitation and detection of

IMM—Instituto de Microelectrónica de Madrid, CSIC, Isaac Newton 8, 28760 Tres Cantos, Madrid, Spain. *e-mail: ricardo.garcia@imm.cnm.csic.es

Table 1 | Cantilever properties.

Eigenmode (flexural)	κ_j	Frequency	Force constant	Quality factor (no internal damping)	Optical sensitivity
j		$\omega_j = \left(\frac{\kappa_j}{\kappa_1}\right)^2 \omega_1$	$k_j = \left(\frac{\omega_j}{\omega_1}\right)^2 k_1$	$Q_j = \frac{\omega_j}{\omega_1} Q_1$	$\sigma_j = \frac{\varphi'_j}{\varphi'_1} \sigma_1$
1	1.875	$\omega_1 = \omega_0$	k_1	Q_1	σ_1
2	4.694	$6.27\,\omega_0$	$39.31\,k_1$	$6.27\,Q_1$	$3.473\,\sigma_1$
3	7.855	$17.55\,\omega_0$	$308\,k_1$	$17.55\,Q_1$	$5.706\,\sigma_1$
4	10.996	$34.39\,\omega_0$	$1183\,k_1$	$34.39\,Q_1$	$7.985\,\sigma_1$

Adapted from refs 26, 32 and 45. The eigenmodes of the AFM cantilever are characterized by four parameters: the effective stiffness k_j (force constant), the resonant frequency $\omega_j = 2\pi f_j$, the quality factor Q_j and the optical sensitivity σ_j. For a rectangular cantilever without a tip there are several relationships among these parameters, which are approximations to describe real AFM cantilevers. κ_j are the real roots of a characteristic equation of the cantilever $(1 + \cos\kappa_j \cosh\kappa_j = 0)$[26]. φ_j is the shape of the jth eigenmode at the free end of the cantilever.

a single frequency component of the tip's motion. Therefore, the information about the properties of a sample that is included in the other frequency components is irreversibly lost.

Multifrequency AFM methods involve the excitation and/or detection of several frequencies of the probe's oscillation. Those frequencies are usually associated with either the higher harmonics of the oscillation or the eigenmodes of the cantilever. Multifrequency excitation/detection schemes provide higher sensitivity and resolution because these methods are specifically designed to decode the information generated by the nonlinear regions of the tip–surface interaction force.

The physics of multifrequency AFM methods

There are two main dynamic AFM methods[3,4,26]. In amplitude-modulation AFM (AM-AFM), the probe is excited at a fixed frequency and the amplitude is held constant by the feedback loop while taking an image. In frequency-modulation AFM (FM-AFM), a single resonant frequency is used for excitation and detection, and the frequency shift is held constant by the feedback loop. The purpose of any dynamic AFM experiment is to recover the information about the sample's properties encoded in the cantilever dynamics. The cantilever dynamics are highly nonlinear[3,18,19,26] because the amplitude of the oscillation is higher than the decay lengths of the interaction forces. For atomic- and molecular-resolution images the decay lengths are about 0.5 nm, whereas the amplitudes are in the range 1–10 nm. To be precise, the nonlinear effects relevant for high-resolution imaging and mapping of material properties are examples of mild nonlinear dynamics. In some situations, the cantilever could experience very complex trajectories[18,19]. But the presence of extreme nonlinear behaviour in force microscopy can be easily avoided by proper selection of the operational parameters.

The presence of several frequency components in the oscillation of the cantilever has been known for several years[27–32]. The role of those components in the spatial resolution and in time-dependent processes and sensitivity to material properties has, however, been either overlooked or neglected because of at least three factors. First, those components were observed by applying large tip–surface forces, which are not suitable for high-resolution imaging[32]. Second, in typical experimental conditions, the higher harmonics components are several orders smaller than the fundamental frequency component[32,33]. To observe them requires either improving the signal-to-noise ratio of the instrument or developing specific experimental methodologies to enhance them. Finally, a comprehensive theory to decode the information about the sample properties in terms of the frequency components is complex and was not initially in place.

The cantilever in an AFM is a mechanical system (Fig. 1). As such it is characterized by its eigenmodes and their respective properties[33–45]. The eigenmodes are also called normal modes or resonances, and are characterized by four parameters: the effective stiffness k_j (force constant), the resonant frequency $\omega_j = 2\pi f_j$, the quality factor Q_j and the optical sensitivity σ_j. For a rectangular cantilever without a tip, there are several relationships among the above parameters (Table 1). The relationships are approximations to describe real AFM cantilevers. The mass of the tip, the presence of a picket-shape at the end of the cantilever, or a non-uniform cantilever's cross-section along its length could introduce significant changes in the mode shape[38,45,46] that would limit the validity of the analytical expressions.

The nonlinearities in the interaction force introduce higher harmonics components in the probe's motion. Thus, the tip–surface force is encoded in the frequency spectra of the tip motion. The harmonics vibrate with a frequency equal to an integer multiple of the excitation frequency ($n\omega$) (Box 1). The amplitude of the

Box 1 | Approximations for the cantilever deflection.

Different degrees of accuracy and complexity can be applied to describe the steady-state deflection of the cantilever. The most common assumption is to consider the expression

$$z = z_0 + A\cos(\omega t - \phi) \quad (1)$$

where A, z_0 and ϕ are, respectively, the amplitude, the static component of the deflection and the phase shift with respect to the driving force. Equation (1) neglects any multifrequency components. The next approximation level considers the presence of high-frequency components (harmonics). The harmonics are naturally generated when the vibrating probe is exposed to the nonlinear regions of the interaction force: then

$$z = z_0 + \sum_{n=1}^{N} A_n \cos(n\omega t - \phi_n) \quad (2)$$

where A_n is the amplitude of the harmonic with angular frequency $n\omega$. Equations (1) and (2) are compatible with a point-mass description of the cantilever.

A more precise description is achieved by considering the extended character of the cantilever. In that case, the deflection of the probe contains contributions from all its eigenmodes (q_j),

$$z = z_0 + \sum_{j=1}^{M} q_j(t) = z_0 + \sum_{n=1}^{N} A_n \cos(n\omega t - \phi_n) \quad (3)$$

In Eq. (3) the eigenmodes have been expressed in terms of the different harmonics (A_n).

Box 2 | The interaction force and the harmonics.

The harmonics and the forces are related by an integral expression. This relationship is obtained by multiplying the equation of motion by $\cos(n\omega t - \phi_n)$ and $\sin(n\omega t - \phi_n)$ and integrating over a period. In amplitude-modulation AFM, the higher harmonics can be expressed as

$$A_n = S\frac{\omega_0}{k}\sqrt{\left|\left(\int_2^T F_{ts}(d)\cos(n\omega t)\mathrm{d}t\right)\right|^2 + \left|\left(\int_2^T F_{ts}(d)\sin(n\omega t)\mathrm{d}t\right)\right|^2} \quad (4)$$

$$S \approx 1/(\pi n^2) \text{ and } n > 3 \quad (5)$$

where d is the instantaneous tip–surface distance. For oscillations where the repulsive region of the interaction potential is stronger than the attractive region, the higher harmonics components can be parameterized in terms of the maximum force (F_{max}) and the contact time t_c:

$$A_n = A_n(F_{max}, t_c, n) \quad (6)$$

In frequency-modulation AFM, the higher harmonics can be expressed in terms of the force by

$$A_n = \frac{2}{\pi k}\frac{1}{1-n^2}\int_{-1}^{1} F_{ts}^n(z_c + z_0 + A_{1u})\frac{T_n(u)}{\sqrt{1-u^2}}\mathrm{d}u \quad (7)$$

where $T_n(u)$ is the nth Chebyshev polynomial of the first kind, z_c is the average position of the cantilever, and $u = \cos \omega t$.

higher harmonics is proportional to the convolution of the force over the harmonic waveform[47] (Box 2). The theoretical analysis also shows that the amplitude of the higher harmonics decreases with the order as $\sim 1/n^2$. When the oscillation amplitude is comparable to the range of the short-range forces, the higher harmonics are proportional to the higher force gradients[48,49].

The higher harmonics act as effective driving forces that excite the vibration of the higher eigenmodes of the cantilever. This happens whenever the frequency of a higher harmonic is close to that of an eigenmode[33,35]. For a rectangular cantilever without a tip, the frequency of the second eigenmode is $6.27\omega_0$, very close to that of the sixth harmonics ($6\omega_0$). As a consequence, the frequency spectra are modulated by the presence of the eigenmodes (Fig. 1e). The above description is supported by both numerical simulations and experimental observations. In liquid, the momentary excitation of the second eigenmode plays a relevant role in the cantilever dynamics[50].

The presence of higher harmonics in the deflection signal allows time-resolved forces to be obtained and thus allows one to measure the sample dynamics in a time frame of microseconds. This method can be divided into two steps[51]. The first step requires the cantilever trajectory to be expressed in the frequency domain. The second step involves taking the inverse Fourier of the cantilever trajectory divided by its transfer function. It requires a relatively large number of harmonics (~15), however, to get accurate estimations of the force. Special cantilevers are required to enhance the number of higher harmonics in the probe's oscillation[46,52,53]. In particular, the development of torsional harmonic cantilevers has improved the signal-to-noise ratio of the higher harmonics and simplified the calculation of the transfer function[54].

The multifrequency aspects of dynamic AFM have been overlooked because the high-frequency components are usually very

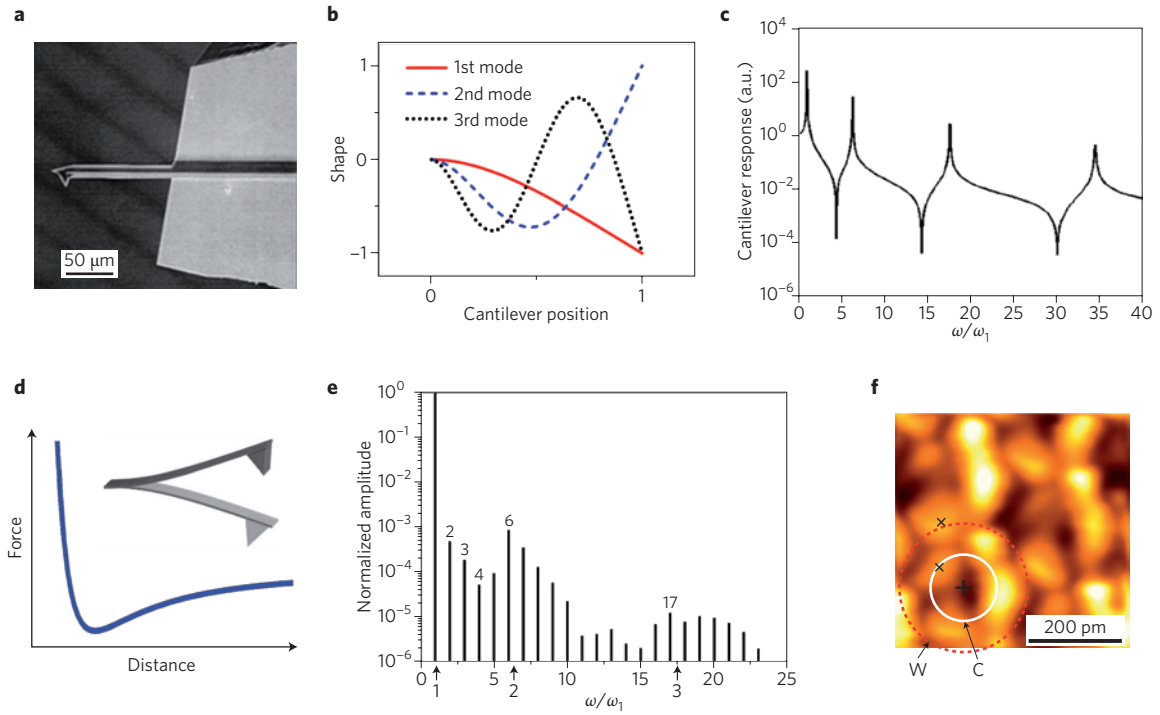

Figure 1 | Cantilever dynamics in force microscopy. a, Scanning electron microscope image of a silicon cantilever. **b**, Modal shapes of the first three flexural eigenmodes of a rectangular (tip-less) cantilever that is clamped at one end and free at the other end. **c**, Amplitude response as a function of the excitation frequency for a rectangular cantilever (simulation). **d**, Schematic diagram of the interaction between a vibrating cantilever and a nonlinear tip–surface force. **e**, Frequency response of a rectangular cantilever under the influence of a nonlinear force (simulation). An enhancement of the amplitudes of the sixth and seventeenth harmonics is observed owing to the coupling, respectively, with the second and third eigenmodes. **f**, Higher harmonic image of a tungsten tip imaging a graphite surface. The four-leaved clover is related to the four-fold symmetry of charge density maxima in a tungsten adatom on W(100). The white and red circles represent the diameter of the carbon and tungston atoms, respectively. Panels reproduced with permission from: **a**,**c**,**e**, ref. 26, © 2010 Wiley; **f**, ref. 48, © 2004 AAAS.

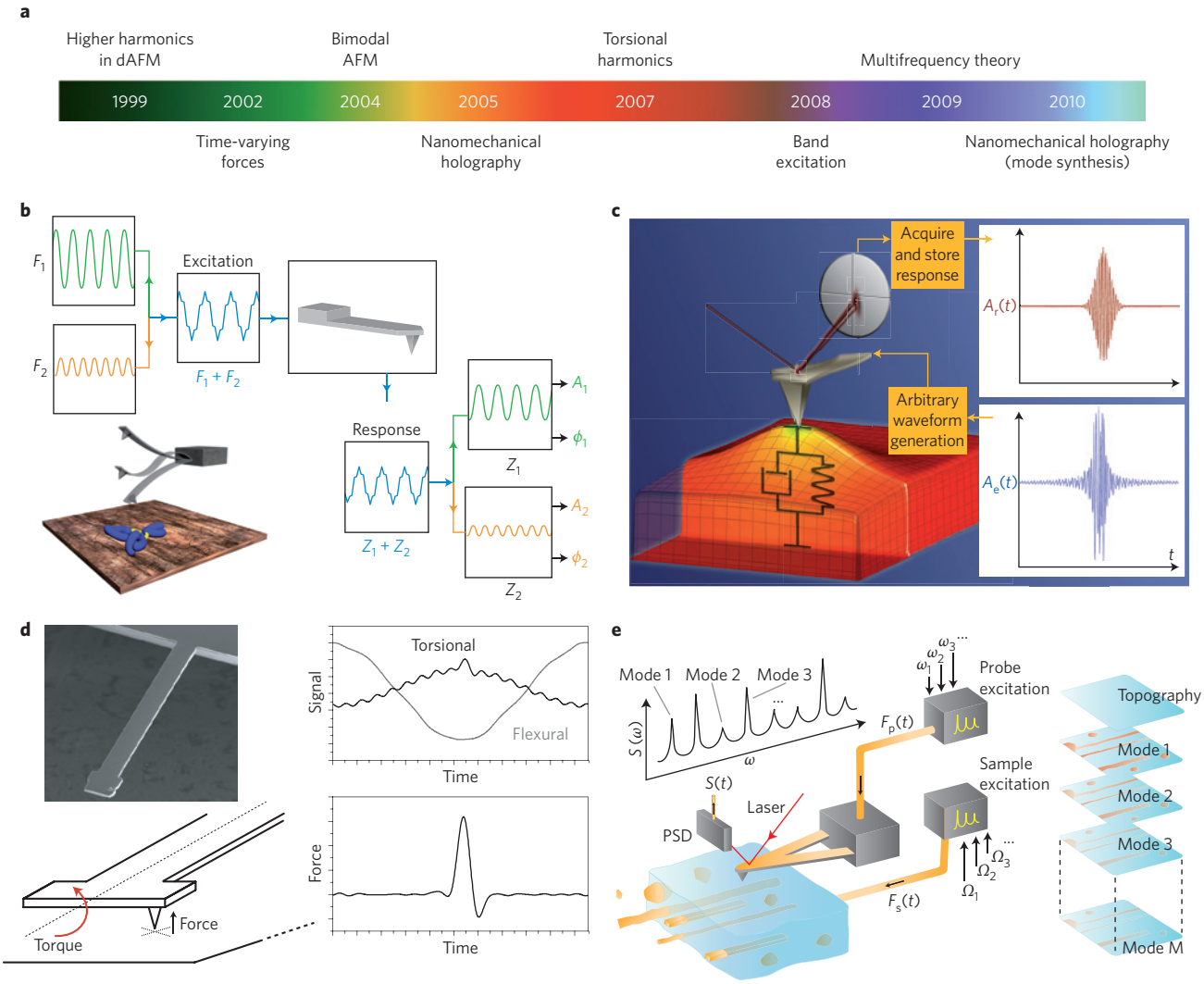

Figure 2 | Multifrequency AFM. a, Milestones in the evolution of multifrequency AFM. **b**, Bimodal AFM scheme. The amplitude of the first mode is used for topography imaging while the signal from the second mode give access to different mechanical or electromagnetic properties. **c**, Schemetic of the band excitation method. The excitation signal is digitally synthesized to have a predefined amplitude and phase in a given frequency window. The cantilever response is detected and Fourier transformed at each pixel in an image. A_r and A_e are the response amplitude and excitation amplitude, respectively. **d**, Scanning electron microscopy image and schematic of a torsional harmonics cantilever. The cantilever is 300 μm long, 3 μm thick and 50 μm wide at the free end. The force is obtained from the higher harmonic components in the torsional signal. **e**, Schematic of a nanomechanical holography set-up. The probe and the sample are mechanically excited by signals that contain a number of known frequency components. From these frequency components, the tip–sample interaction synthesizes new modes (*S* signal), which carry information on the subsurface structures. PSD; photo segmented diode. F_p and F_s are the excitation force of the probe and the excitation force of the sample, respectively. Ω represents the excitation frequencies of the sample. Panels reproduced with permission from: **b**, ref. 56, © 2008 IOP; **c**, ref. 65, © 2007 IOP; **d**, ref. 54, © 2007 NPG; **e**, ref. 106, © 2010 NPG.

small. For example, it has been shown that for high-Q cantilevers ($Q \geq 50$), the amplitudes of the higher harmonics are two to three orders of magnitude smaller than the fundamental component[33]. The amplitude of the higher eigenmodes can be enhanced by exciting several of them simultaneously, the simplest case being the excitation of the first two eigenmodes[55–57]. By recording the signal at the excited frequencies, one can acquire complementary information on the sample properties from different channels, one per excited eigenmode[58–61]. This approach has several advantages. For example, in AM-AFM the feedback imposes considerable restrictions on the information conveyed by the phase shift of the mode used by the feedback frequency. Those restrictions do not apply to the information carried by the second excited eigenmode[60]. In addition, the simultaneous excitation of two modes enhances the coupling of those modes by the nonlinear force. This helps to increase the sensitivity of the second mode to material properties[56]. For small amplitudes, the parameters of the second mode can be related to the force gradient[58,61], which also explains the higher sensitivity of bimodal AFM to variations in material properties.

This approach has been extended to the simultaneous excitation of three eigenmodes[62] and to non-resonant frequencies, for example to two frequencies that are in the vicinity of a resonance[63,64]. In the latter case, the tip–surface forces generate a new set of frequencies called intermodulation products[63] which also encode the interaction force. There are other remarkable results produced by the simultaneous excitation of several frequencies near the fundamental resonance, such as the real-time determination of the

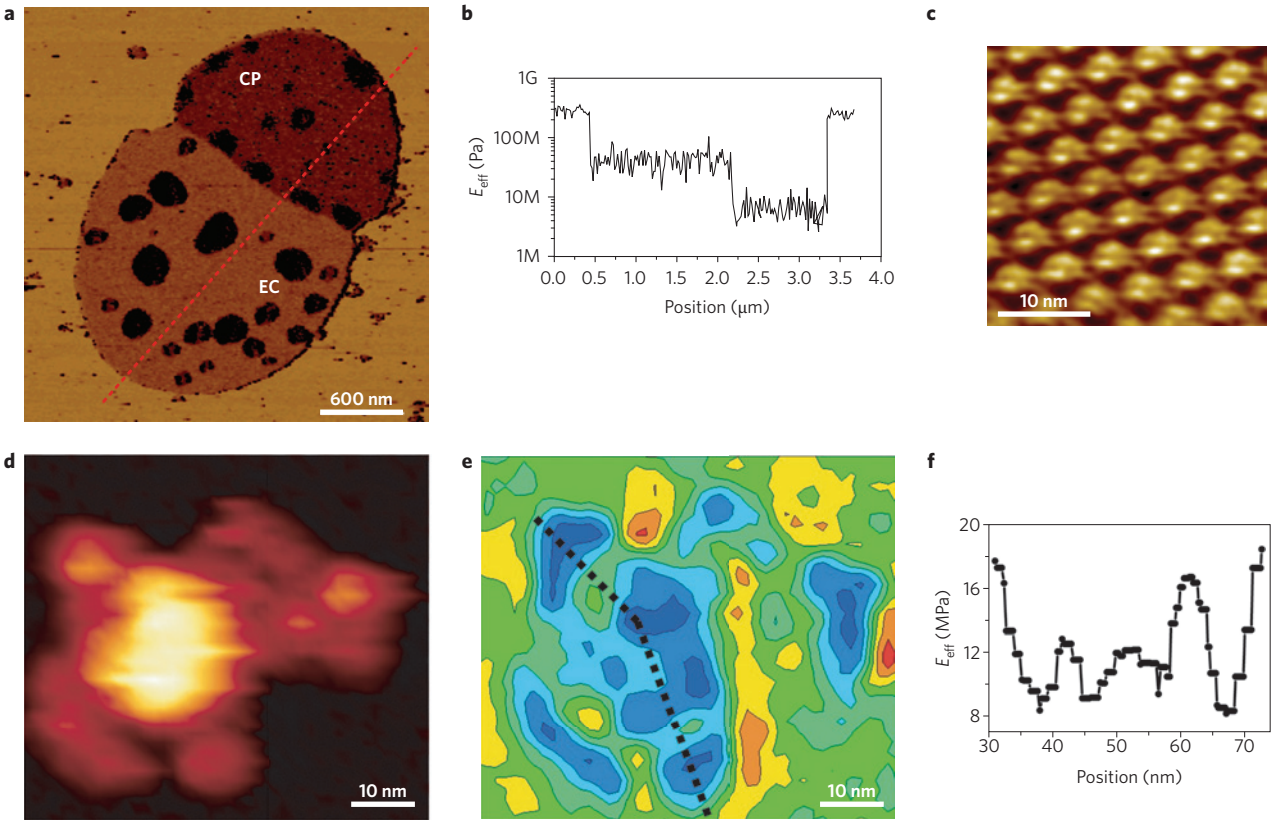

Figure 3 | Topography and flexibility mapping of proteins. a, Flexibility map of a purple membrane sheet showing extracellular (EC) and cytoplasmatic (CP) sides. **b**, The cross-section shows the variations along the line marked in **a**. **c**, High-resolution flexibility image of a region of the EC side. The image shows the protein trimers arranged in a lattice with a parameter of 6 nm. The contrast arises from changes in the elasticity between the protein and lipid regions. **d**, Bimodal AFM topography. **e**, Flexibility map of a single immunoglobulin M antibody taken simultaneously with **d**. The scale of the effective elastic (Young) modulus goes from blue (lowest values) to red (highest values). The image was obtained by applying very small forces (40 pN). **f**, Flexibility profile along the dashed line marked in **e**. The profile shows local variations in the flexibility that are consistent with the orientation flexibility of the antibody complex when its binds a cell surface antigen. Panels reproduced with permission from: **a**–**c**, ref. 93, © 2009 NPG; **d**–**f**, ref. 61, © 2011 APS.

effective cantilever parameters[65,66] or the control of some nonlinear dynamics properties[67,68].

The use of higher flexural eigenmodes for imaging (single excitation/detection) has been suggested to avoid the jump-to-contact phenomenon[69–71]. However, the higher the eigenmode the lower the sensitivity to the properties of a material. The sensitivity of a mode depends on the Q_j/k_j ratio[72] which, for an ideal cantilever, decreases with the eigenmode order (Table 1).

Multifrequency AFM methods

There are currently five approaches to multifrequency AFM that are widely used (Fig. 2).

Multiharmonic AFM imaging. This is the most straightforward approach to performing a multifrequency AFM experiment. It requires just the recording and subsequent plotting of the higher harmonics components generated while acquiring a topography image in conventional dynamic AFM modes[73–80]. However, the detection of higher harmonics in air is hard to achieve with the forces required for high-resolution imaging[6,8] (which may be less than 1 nN). For this reason the use of special cantilevers that allowed the tuning of a higher eigenmode with a higher harmonic has been suggested[46]. The fact that in liquid the higher harmonics are easier to detect has allowed the imaging of a bacterial S-layer with 0.5 nm spatial resolution by plotting the amplitude of the second harmonic of the fundamental frequency[78]. The same method has been applied to image a living bacterium[79] with an enhancement in contrast. The combination of several harmonics, in particular the zeroth, first and second harmonics, has allowed nanoscale mapping of the local stiffness and viscoelastic dissipation in living cells[80]. In ultrahigh vacuum, the use of higher harmonics has revealed features with a lateral distance of only 77 pm on a tungsten surface[48].

Bimodal AFM. This method uses two driving forces to excite the vibration of the cantilever[55–58,81] (Fig. 2b). The excitation frequencies are tuned to match two of the flexural eigenmodes of the cantilever, usually the first and the second eigenmodes. An output signal of the first mode (either the amplitude or the frequency shift) is used to image the topography of the surface while the output signals of the second mode (amplitude and/or phase shift) are used to measure changes in mechanical[81–85], magnetic[72,86] or electrical properties[87,88] of the surface. This method is compatible with both dynamic AFM modes and can be performed in air[81], liquid[56,57] or ultrahigh vacuum[58,89]. Bimodal AFM has been operated at very low forces (50 pN) in liquid, allowing the non-invasive imaging of isolated proteins[61].

Bimodal AFM offers a straightforward approach to separate topography from other interactions influencing the tip motion such as magnetic or electrostatic forces. Thus, the different resonances of the cantilever could be seen as channels to access and

Box 3 | Simultaneous topography and flexibility mapping.

In bimodal AFM the motion of the tip can be approximated as

$$z = z_0 + q_1(t) + q_2(t) = z_0 + A_1 \cos(\omega_1 t - \phi_1) + A_2 \cos(\omega_2 t - \phi_2) \quad (8)$$

where A_j and ϕ_j are the amplitudes and phase shifts of the excited modes, respectively. The application of the virial theorem to the free eigenmode (the second) in bimodal AFM gives a relationship between the parameters of the second mode and the gradient of the interaction force. Then, by applying contact mechanics, the sample flexibility can be obtained in terms of the amplitude and phase shift of the second mode. From the virial theorem it is deduced ($A_{02} << A_{01}$)

$$\frac{dF_{ts}}{dz}(d) \approx C\frac{k_2 A_{02}}{Q_2 A_2}\cos\phi_2 \quad (9)$$

where A_{02}, k_2 and Q_2 are, respectively, the free amplitude, force constant and quality factor of the second eigenmode, and C is a correction factor that converges to a constant value for high A_{01}/A_{02} ratios. Finally, by applying the Hertz contact mechanics model,

$$\frac{dF_{ts}}{dz} = 2E_{eff}a \quad (10)$$

where a is the contact radius and E_{eff} is the flexibility (effective elastic modulus).

separate different sample properties. To avoid the excitation of non-periodic oscillations, some restrictions must be set on the values of the amplitude ratio between the excited resonances[56,84].

Band excitation. This method introduces a synthesized digital signal that spans a continuous band of frequencies, and monitors the response within the same or even larger frequency band[65,90,91]. The method aims to improve the ability to acquire different dynamic curves while the topography of the surface is recorded. The cantilever response is detected using high-speed data acquisition methods and then Fourier transformed. The resulting amplitude–frequency and phase–frequency curves are collected at each point of the surface and stored in three-dimensional data arrays. These data are analysed to extract some of the relevant parameters that characterize the cantilever behaviour (Fig. 2c). For example, in the single harmonic oscillator approximation, the resonant frequencies, the amplitude and Q are deconvolved and stored as images. Furthermore, in the case of adaptive control the data can be used as a feedback signal in microscope operation.

Band excitation has been applied to probe the electromechanical coupling in soft biological systems by distinguishing among damping, Young modulus and electromechanical contributions. Notably, it has also been used to study ion diffusion in electrochemical batteries[90,91]. The large amount of data generated in a band excitation experiment together with the need for sophisticated controllers might, however, become major obstacles for a wide use of this approach.

Torsional harmonic AFM. This is an approach based on the recording of the higher harmonics of the torsional signal[54,92,93]. Torsional harmonic AFM can be used to generate a topographic image of the sample surface while the time-varying forces are recorded. The topographic image is a conventional AM-AFM image. At the same time, the tip–surface force is obtained by integrating the higher harmonics of the torsional signal. Torsional harmonic AFM requires the use of specially designed cantilevers where the tip is offset from the cantilever axis (Fig. 2d). This design favours the existence of a torque around the axis of the cantilever, which enhances the presence of the large number of higher harmonics needed for an accurate calculation of the time-varying force[92]. From those forces it is possible to measure locally some mechanical properties, such as the Young modulus[93]. Remarkably, those measurements have also been applied to detect and quantify DNA molecules[94] and to measure molecular recognition processes[95]. Torsional harmonic AFM measurements have revealed significant differences in the fractal dimensionality of cancerous cells with respect to normal cells[96]. These measurements underline the potential of multifrequency AFM in nanomedicine.

Nanomechanical holography. This technique combines elements derived from ultrasonic[97,98] and dynamic force microscopies[3] to generate images of structures that lie below the surface of biological or synthetic materials[99,100]. It is based on the simultaneous excitation of the sample and the probe[99–103]. The mechanical excitation of the sample generates waves that propagate through the sample. Those waves are scattered by the internal features or structures of the material. As a consequence, the amplitude and the phase shift of the waves are modified, the modification depending on the local mechanical properties of the features. Eventually the scattered waves emerge on the surface where they influence the tip–surface coupling.

In some cases, the coupling of the sample and the vibrations of the cantilever generates a new set of frequencies that are a linear combination of the frequencies used to excite the tip and the sample, the simplest case being the difference between them. An image of the subsurface structure is acquired by plotting the phase shift of one of the synthesized modes as the probe moves across the sample surface. Nanomechanical holography has been applied to image the inner structure of different cells[99,100], and in particular the presence of nanoparticles inside soft materials[101] or in the lung cells of mice exposed to single-walled carbon nanohorns[102]. It is also applied to investigate the dimensionality and fatigue performance of buried electrical contacts and interconnects in microelectronics devices[103]. But difficulties in interpreting the images in terms of the properties of the subsurface structures pose challenges for the progress of the technique.

Applications

Multifrequency AFM methods have been used in a range of different fields, from energy storage to nanomedicine, and can investigate properties that are not easily accessible by conventional AFM methods.

Mapping protein flexibility with molecular resolution. Protein flexibility plays a central role in binding to other proteins either isolated or embedded in a membrane as cell receptors. Current methods for the determination of the protein flexibility give results on a timescale of picoseconds that might not be relevant to the speed at which proteins undergo conformational changes in physiological conditions (micro- to milliseconds). Multifrequency AFM methods have measured, with molecular resolution, the flexibility of several proteins in liquid (Fig. 3). Torsional harmonic AFM has mapped the flexibility of proteins in purple membrane sheets at the microsecond timescale by monitoring surface-induced deformations[93] (Fig. 3a–c). The measurements show differences in the flexibility between the cytoplasmatic (4–10 MPa) and extracellular sides (15–50 MPa) of the membrane.

Complementary experiments have been performed with a bimodal AFM by mapping the topography and the flexibility of isolated proteins in physiological conditions[61] (Fig. 3d–f). The images

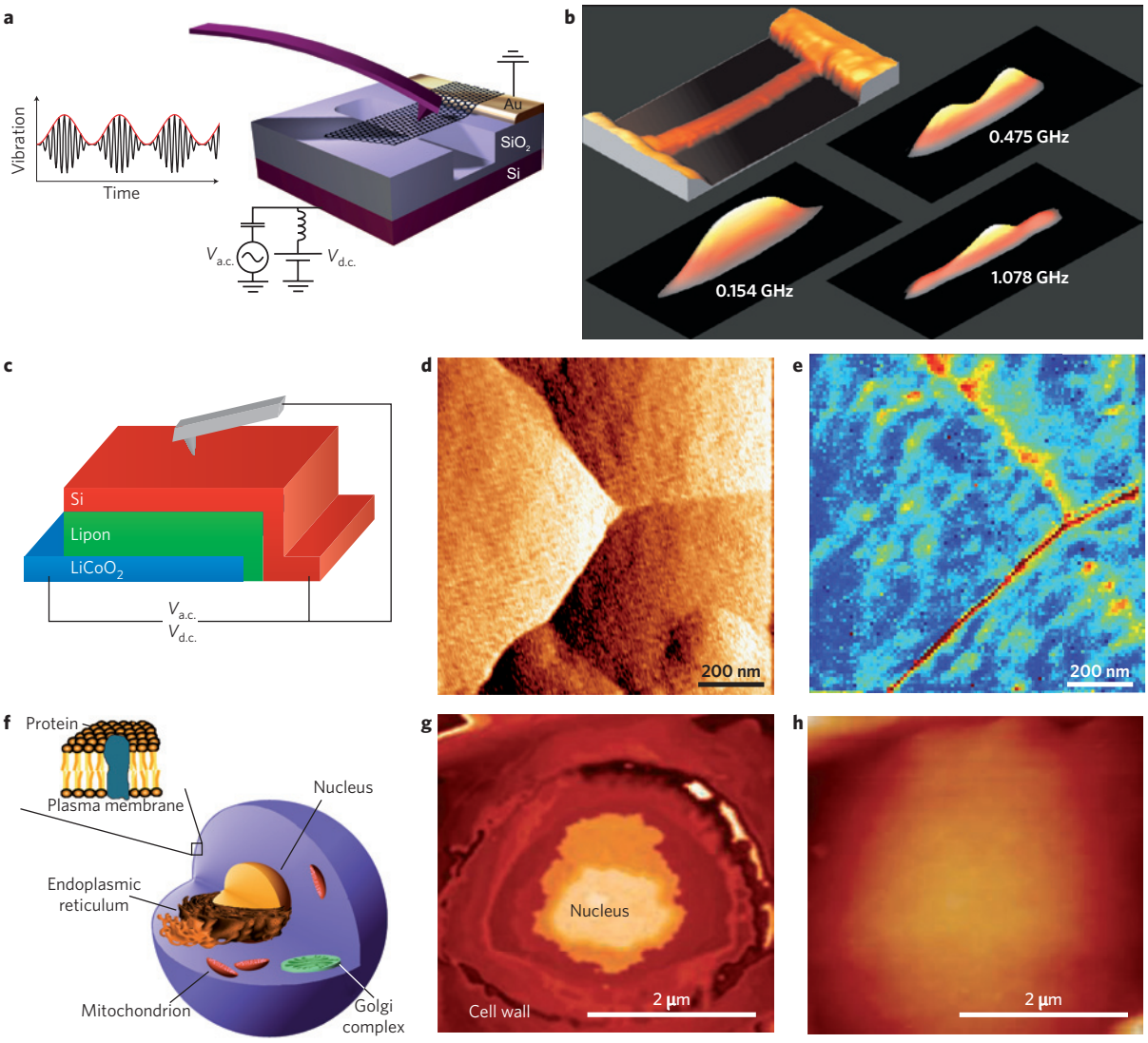

Figure 4 | Mapping high-frequency oscillations, ion diffusion and subsurface structures. a, Scheme to image the spatial shape of vibrations in nanoscale resonators. A signal modulated at the frequency of the first eigenmode of the cantilever is used to excite the resonator. **b**, Spatial shape of the first three modes of a carbon nanotube suspended between two gold electrodes. **c**, Schematic of the band excitation experiment to measure ion diffusion in a battery. Lipon is the electrolyte; it stands for lithium phosphorus oxynitride. **d**, AFM deflection image of grain interfaces in the electrode. **e**, Images of the regions that concentrate the lithium ions (in red) during battery charging. **f**, Cross-section of a cell. **g**, Nanomechanical holography image of a mouse cell. **h**, Conventional AFM image of the same cell. Panels reproduced with permission from: **a**, ref. 105, © 2008 ACS; **b**, ref. 104, © 2007 APS; **c–e**, ref. 91, © 2010 ACS; **g**,**h**, ref. 107, © G. S Shekhawat and V. P. Dravid, Northwestern Univ.

of single proteins (antibodies) have been obtained non-invasively because the bimodal approach in combination with FM-AFM enables imaging under the application of very small forces (below 50 pN). Figure 3d shows the topography of a single protein complex and Fig. 3e the corresponding flexibility map (local variations of the elastic modulus; see Box 3). The flexibility map shows a maximum of 19 MPa and a minimum value of 8.2 MPa. The comparison between the flexibility map and the structure of the protein complex shows that the uppermost part is stiffer, probably as a consequence of the presence of intermolecular disulphide bonds joining different fragments of the protein complex. On the other hand, low values of the elastic modulus are found in the last domain of the antigen-binding arms. The above findings are consistent with the orientation flexibility of the antibody complex when it binds a cell-surface antigen.

Imaging the mechanical vibrations of carbon-based resonators. Carbon nanotubes and graphene sheets have been used to fabricate mechanical resonators that can be operated at ultrahigh frequencies, have tunable resonance frequencies, and can be used as ultrasensitive inertial mass sensors[24,25,104]. A variation of the bimodal AFM approach has been implemented to detect, identify and image the spatial shape of the eigenmodes of these resonators[104,105] (Fig. 4a,b). This method has enabled the observation of a new class of exotic nanoscale vibration eigenmodes not predicted by the elastic beam theory, where the amplitude of vibration is a maximum at the free edges[105]. The motion of the suspended resonators was electrostatically driven by applying a voltage (V_{RF}). Because the resonances of nanoscale resonators are far above the mechanical response of AFM cantilevers, the excitation voltage of the resonators was modulated at the frequency of the first eigenmode of the cantilever (Fig. 4a). The mechanical vibrations were detected and imaged by following the changes of the envelope of the vibration amplitude. Figure 4b shows an AFM image of a suspended carbon nanotube and its first three eigenmodes.

Mapping ion diffusion. Lithium-ion batteries are common in applications such as mobile electronic devices and electric and hybrid vehicles. The movement of lithium ions into and out of electrodes is central to the operation of those batteries. However, this displacement has not been described at the nanoscale, and this limits the understanding of the mechanisms underpinning lithium-ion battery operation. Band excitation experiments (Fig. 4c–e) have demonstrated the existence of a strong coupling between lithium-ion concentration and cathode lattice parameters[90,91] and have established that the diffusion coefficient increases for certain grain orientations and single-grain boundaries (red regions in Fig. 4e). The lateral resolution of ~20 nm allows lithium-ion motion to be probed in volumes 10^6 times smaller than possible by classical current-based electrochemical methods. These results offer a direct path to improving the electrochemical performance of lithium-ion batteries. In the above measurements the sensitivity of the band excitation method enabled measurement of the changes in the lattice parameter associated with the ion diffusion and migration.

Subsurface imaging in cells. Imaging structures beneath the surface of a sample with sub-100-nm spatial resolution has always been a formidable challenge in microscopy. Typically, high-resolution images of a subsurface structure are obtained by slicing the material and observing the newly created surface, but this approach damages the sample under study. Nanomechanical holography has demonstrated its potential for the non-destructive imaging of embedded or buried substructures of several animal and plant cells[99,100]. Remarkably, those experiments have been performed without any labelling or sectioning of cells, and under physiologically viable conditions. Figure 4g shows a nanomechanical holography image taken simultaneously with a conventional AFM image (Fig. 4h). Several features of the cell substructure (Fig. 4f) such as the cell walls and the nucleus are resolved in the image. In comparison, the conventional AFM image shows a featureless object.

Summary and outlook

Force microscopy is evolving from a technique that involves the excitation and detection of a single frequency to one that involves multiple frequencies. This development is being driven by a variety of factors. In some cases, there is a need to operate the instrument under very low forces. In others, there is a need to improve the spatial resolution of soft materials or to measure surface properties without compromising fast data acquisition times. There is also a drive to find new applications in fields such as materials science or nanomedicine.

Multifrequency AFM can be thought of as a new field in force microscopy. This is due to the diversity of multifrequency approaches available, the use of new excitation or detection schemes, and the emphasis placed on mixing several frequencies. This new field provides a promising framework to improve compositional sensitivity and spatial and time resolution of materials in their native environment and, at the same time, allows properties that are not accessible to conventional force microscopes to be measured. Multifrequency AFM methods are conceptually more demanding than conventional AFM methods, but this would seem to be a reasonable price to pay to sustain the impressive development of force microscopy that has been seen over the past 25 years.

References

1. Binnig, G., Quate, C. F. & Gerber, C. Atomic force microscope. *Phys. Rev. Lett.* **56,** 930–933 (1986).
2. Meyer, G. & Amer, N. M. Novel optical approach to atomic force microscopy. *Appl. Phys. Lett.* **53,** 1045–1047 (1988).
3. Garcia, R. & Perez, R. Dynamic atomic force microscopy methods. *Surf. Sci. Rep.* **47,** 197–301 (2002).
4. Giessibl, F. J. Advances in atomic force microscopy. *Rev. Mod. Phys.* **75,** 949–983 (2003).
5. Parot, P. *et al.* Past, present and future of atomic force microscopy in life sciences and medicine. *J. Mol. Recognit.* **20,** 418–431 (2007).
6. Garcia, R., Magerle, R. & Perez, R. Nanoscale compositional mapping with gentle forces. *Nature Mater.* **6,** 405–411 (2007).
7. Ando, T., Uchihashi, T. & Fukuma, T. High-speed atomic force microscopy for nano-visualization of dynamic biomolecular processes. *Prog. Surf. Sci.* **83,** 337–437 (2008).
8. Gan, Y. Atomic and subnanometer resolution in ambient conditions by atomic force microscopy. *Surf. Sci. Rep.* **64,** 99–121 (2009).
9. Klinov, D. & Magonov, S. True molecular resolution in tapping-mode atomic force microscopy with high-resolution probes. *Appl. Phys. Lett.* **84,** 2697–2699 (2004).
10. Fukuma, T., Kobayashi, K., Matsushige, K. & Yamada, H. True atomic resolution in liquid by frequency-modulation atomic force microscopy. *Appl. Phys. Lett.* **87,** 034101 (2005).
11. Yamada, H. *et al.* Molecular resolution imaging of protein molecules in liquid using frequency modulation atomic force microscopy. *Appl. Phys. Lett.* **2,** 095007 (2009).
12. Higgings, M. J., Sader, J. E. & Jarvis, S. P. Frequency modulation atomic force microscopy reveals individual intermediates with each unfolded I27 titin domain. *Biophys. J.* **90,** 640–647 (2006).
13. Kuna, J. J. *et al.* The effect of nanometre-scale structure on interfacial energy. *Nature Mater.* **8,** 837–842 (2009).
14. Baykara, M. Z., Schwendemann, T. C., Altman, E. I. & Schwarz, U. D. Three-dimensional atomic force microscopy: taking surface imaging to the next level. *Adv. Mater.* **22,** 2838–2853 (2010).
15. Palermo, V., Palma, M. & Samori, P. Electronic characterization of organic thin films by Kelvin probe force microscopy. *Adv. Mater.* **18,** 145–164 (2006).
16. Schwarz, A. & Wiesendanger, W. Magnetic sensitive force microscopy. *Nano Today* **3,** 28–39 (2008).
17. Luan, B. & Robbins, M. O. Contact of single asperities with varying adhesion: comparing continuum mechanics to atomistic simulations. *Phys. Rev. E* **74,** 026111 (2006).
18. Raman, A., Melcher, J. & Tung, R. Cantilever dynamics in atomic force microscopy. *Nano Today* **3,** 20–27 (2008).
19. Stark, R. W. Bistability, higher harmonics and chaos in AFM. *Mater. Today* **13,** 24–32 (September 2010).
20. Butt, H. J., Capella, B. & Kappl, M. Force measurements with the atomic force microscope: technique, interpretation and applications. *Surf. Sci. Rep.* **59,** 1–152 (2005).
21. Bizarri, A. R. & Cannistraro, S. The application of atomic force spectroscopy to the study of biological complexes undergoing a biorecognition process. *Chem. Soc. Rev.* **39,** 734–749 (2010).
22. Cross, S. E., Jin, Y-S., Rao, J. & Gimzewski, J. K. Nanomechanical analysis of cells from cancer patients. *Nature Nanotech.* **2,** 780–783 (2007).
23. Goetz, J. G. *et al.* Biomechanical remodeling of the microenvironment by stromal caveolin-1 favors tumor invasion and metastasis. *Cell* **146,** 148–163 (2011).
24. Arlett, J. L., Myers, E. B. & Roukes, M. L. Comparative advantages of mechanical biosensors. *Nature Nanotech.* **6,** 203–215 (2011).
25. Gil-Santos, E. *et al.* Nanomechanical mass sensing and stiffness spectrometry based on two-dimensional vibrations of resonant nanowires. *Nature Nanotech.* **5,** 641–645 (2010).
26. Garcia, R. *Amplitude Modulation Atomic Force Microscopy* (Wiley, 2010).
27. Butt, H. J. & Jascke, M. Calculation of thermal noise in atomic force microscopy. *Nanotechnology* **6,** 1–7 (1995). **This paper calculates the thermal noise of the cantilever by including the contributions from all the cantilever eigenmodes.**
28. Rabe, U., Turner, I. & Arnold, W. Analysis of the high-frequency response of atomic force microscope levers. *Appl. Phys. A* **66,** S277–S282 (1998).
29. Sader, J. E. Frequency response of cantilever beams immersed in viscous fluids with applications to the atomic force microscope. *J. Appl. Phys.* **84,** 64–76 (1998).
30. Dürig, U. Relations between interaction force and frequency shift in large-amplitude dynamic force microscopy. *Appl. Phys. Lett.* **75,** 433–435 (1999).
31. Tamayo, J. Energy dissipation in tapping-mode scanning force microscopy with low quality factors. *Appl. Phys. Lett.* **75,** 3569–3571 (1999).
32. Stark, R. W. & Heckel, W. M. Fourier transformed atomic force microscopy: tapping mode atomic force microscopy beyond the Hookian approximation. *Surf. Sci.* **457,** 219–228 (2000).
33. Rodriguez, T. R. & Garcia, R. Tip motion in amplitude modulation (tapping-mode) atomic-force microscopy: comparison between continuous and point-mass models. *Appl. Phys. Lett.* **80,** 1646–1648 (2002).

34. Rabe, U., Janser, K. & Arnold, W. Vibrations of free and surface-coupled atomic force microscope cantilevers: theory and experiment. *Rev. Sci. Instrum.* **67,** 3281–3293 (1996).
35. Stark, R. W., Schitter, G., Stark, M., Guckenberger, R. & Stemmer, A. State-space model of freely vibrating and surface-coupled cantilever dynamics in atomic force microscopy. *Phys. Rev. B* **69,** 085412 (2004).
36. Schaffer, T. E. & Fuchs, H. Optimized detection of normal vibration modes of atomic force microscope cantilevers with the optical beam deflection method. *J. Appl. Phys.* **97,** 083524 (2005).
37. Hsu, J. C., Lee, H. L. & Chang, W. J. Flexural vibration frequency of atomic force microscope cantilevers using Timoshenko beam theory. *Nanotechnology* **18,** 285503 (2007).
38. Melcher, J., Hu, S. & Raman, A. Equivalent point-mass models of continuous atomic force microscope probes. *Appl. Phys. Lett.* **91,** 053101 (2007).
39. Cantrell, J. H. & Cantrell, S. A. Analytical model of the nonlinear dynamics of cantilever tip–sample surface interactions for various acoustic atomic force microscopies. *Phys. Rev. B* **77,** 165409 (2008).
40. Kokavecz, J. & Mechler, A. Spring constant of microcantilevers in fundamental and higher eigenmodes. *Phys. Rev. B* **78,** 172101 (2008).
41. Hahner, G. Dynamic spring constants for higher flexural modes of cantilever plates with applications to atomic force microscopy. *Ultramicroscopy* **110,** 801–806 (2010).
42. Zypman, F. Internal damping for noncontact atomic force microscopy cantilevers. *J. Vac. Sci. Technol. B* **28**, C4E24–C4E27 (2010).
43. Abbasi, M. & Mohammadi, A. K. A new model for investigating the flexural vibration of an atomic force microscope cantilever. *Ultramicroscopy* **110,** 1374–1379 (2010).
44. Pishkenari, H. N. & Meghdari, A. Effects of higher oscillation modes on TM-AFM measurements. *Ultramicroscopy* **111,** 107–116 (2011).
45. Kiracofe, D. & Raman, A. On eigenmodes, stiffness, and sensitivity of atomic force microscope cantilevers in air versus liquids. *J. Appl. Phys.* **107,** 033506 (2009). **Theoretical and experimental study of the influence of the tip mass on the sensitivity and stiffness of the cantilever eigenmodes**.
46. Sahin, O. *et al.* High-resolution imaging of elastic properties using harmonic cantilevers. *Sensor Actuat. A* **114,** 183–190 (2004).
47. Dürig, U. Interaction sensing in dynamic force microscopy. *New J. Phys.* **2,** 5.1–5.12 (2000).
48. Hembacher, S., Giessibl, F. J. & Mannhart, J. Force microscopy with light-atom probes. *Science* **305,** 380–383 (2004). **First experimental result reporting the use of higher harmonics to enhance spatial resolution in force microscopy**.
49. Wright, C. A. & Solares, S. D. On mapping subangstrom electron clouds with force microscopy. *Nano Lett.* **11,** 5026–5033 (2011).
50. Xu, X., Melcher, J., Basak, S., Reinferberger, R. & Raman, A. Compositional contrast of biological materials in liquids using the momentary excitation of higher eigenmodes in dynamic AFM. *Phys. Rev. Lett.* **102,** 060801 (2009).
51. Stark, M., Stark, R. W., Heckl, W. H. & Guckenberger, R. Inverting dynamic force microscopy: From signals to time-resolved interaction forces. *Proc. Natl Acad. Sci. USA* **99,** 8473–8478 (2002). **Method to obtain time-resolved forces by recording the frequency spectra (higher harmonics) of the tip motion**.
52. Sarioglu, A. F. & Solgaard, O. Modeling, design, and analysis of interferometric cantilevers for time-resolved force measurements in tapping-mode atomic force microscopy. *J. Appl. Phys.* **109,** 064316 (2011).
53. Parlak, Z. & Degertekin, F. L. Combined quantitative ultrasonic and time-resolved interaction force AFM imaging. *Rev. Sci. Instrum.* **82,** 013703 (2011).
54. Sahin, O., Quate, C. F., Solgaard, O. & Atalar, A. An atomic force microscope tip designed to measure time-varying nanomechanical forces. *Nature Nanotech.* **2,** 507–514 (2007). **Measurement of time-resolved forces by using the higher harmonics of the torsional cantilever deflection**. **Torsional higher harmonics are easier to measure than those in the flexural deflection**.
55. Rodriguez, T. R. & Garcia, R. Compositional mapping of surfaces in atomic force microscopy by excitation of the second normal mode of the cantilever. *Appl. Phys. Lett.* **84,** 449–451 (2004). **Numerical simulation-based study to enhance the force sensitivity in AFM by the simultaneous excitation of two eigenmodes**. **These simulations provided the framework for development of bimodal AFM**.
56. Martinez, N. F. *et al.* Bimodal atomic force microscopy imaging of isolated antibodies in air and liquid. *Nanotechnology* **19,** 384011 (2008).
57. Proksch, R. Multifrequency, repulsive-mode amplitude-modulated atomic force microscopy. *Appl. Phys. Lett.* **89,** 113121 (2006).
58. Kawai, S. *et al.* Systematic achievement of improved atomic-scale contrast via bimodal dynamic force microscopy. *Phys. Rev. Lett.* **103,** 220801 (2009).
59. Aksoy, M. D. & Atalar, A. Force spectroscopy using bimodal frequency modulation atomic force microscopy. *Phys. Rev. B* **83,** 075416 (2011).
60. Lozano, J. R. & Garcia, R. Theory of multifrequency AFM. *Phys. Rev. Lett.* **100,** 076102 (2008).
61. Martinez-Martin, D., Herruzo, E. T., Dietz, C., Gomez-Herrero, J. & Garcia, R. Noninvasive protein structural fexibility mapping by bimodal dynamic force microscopy. *Phys. Rev. Lett.* **106,** 198101 (2011).
62. Solares, S. D. & Chawla, G. Frequency response of higher cantilever eigenmodes in bimodal and trimodal tapping mode atomic force microscopy. *Meas. Sci. Technol.* **21,** 125502 (2010).
63. Platz, D., Tholén, E. A. & Haviland, D. B. Intermodulation atomic force microscopy. *Appl. Phys. Lett.* **92,** 153106 (2008).
64. Hutter, C., Platz, D., Tholen, E. A., Hansson, T. H. & Haviland, D. B. Reconstructing nonlinearities with intermodulation spectroscopy. *Phys. Rev. Lett.* **104,** 050801 (2010).
65. Jesse, S., Kalinin, S. V., Proksch, R., Baddorf, A. P. & Rodriguez, B. J. Energy dissipation measurements on the nanoscale: band excitation method in scanning probe microscopy. *Nanotechnology* **18,** 435503 (2007).
66. Agarwal, P. & Salapaka, M. V. Real time estimation of equivalent cantilever parameters in tapping mode atomic force microscopy. *Appl. Phys. Lett.* **95,** 083113 (2009).
67. Thota, P., MacLaren, S. & Dankowitz, H. Controlling bistability in tapping mode atomic force microscopy using dual-frequency excitation. *Appl. Phys. Lett.* **91,** 093108 (2007).
68. Dick, A. J. & Solares, S. D. Utilizing off-resonance and dual-frequency excitation to distinguish attractive and repulsive surface forces in atomic force microscopy. *J. Comp. Nonlin. Dyn.* **6,** 031005 (2011).
69. Kawai, S., Kitamura, S., Kobayashi, D., Meguro, S. & Kawakatsu, H. An ultrasmall amplitude operation of dynamic force microscopy with second flexural mode. *Appl. Phys. Lett.* **86,** 193107 (2005).
70. Killgore, J. P., Kelly, J. Y., Stafford, C. M., Fasolka, M. J. & Hurley, D. C. Quantitative subsurface contact resonance force microscopy of model polymer nanocomposites. *Nanotechnology* **22,** 175706 (2011).
71. Pfeiffer, O. *et al.* Using higher flexural modes in non-contact force microscopy. *Appl. Surf. Sci.* **157,** 337–342 (2000).
72. Dietz, C., Herruzo, E. T., Lozano, J. R. & Garcia, R. Nanomechanical coupling enables detection and imaging of 5 nm superparamagnetic particles in liquid. *Nanotechnology* **22,** 125708 (2011).
73. Stark, M., Stark, R. W., Heckl, W. M. & Guckenberger, R. Spectroscopy of the anharmonic cantilever oscillations in tapping-mode atomic-force microscopy. *Appl. Phys. Lett.* **77,** 3293–3295 (2000).
74. Sahin, O., Quate, C. F., Solgaard, O. & Atalar, A. Resonant harmonic response in tapping-mode atomic force microscopy. *Phys. Rev. B* **69,** 165416 (2004).
75. Crittenden, S., Raman, A. & Reifenberger, R. Probing attractive forces at the nanoscale using higher-harmonic dynamic force microscopy. *Phys. Rev. B* **72,** 235422 (2005).
76. Balantekin, M. & Atalar, A. Enhancing higher harmonics of a tapping cantilever by excitation at a submultiple of its resonance frequency. *Phys. Rev. B* **71,** 125416 (2005).
77. Legleiter, J., Park, M., Cusick, B. & Kowalewski, T. Scanning probe acceleration microscopy (SPAM) in fluids: mapping mechanical properties of surfaces at the nanoscale. *Proc. Natl Acad. Sci. USA* **103,** 4813–4818 (2006).
78. Preiner, J., Tang, J., Pastushenko, V. & Hinterdorfer, P. Higher harmonic atomic force microscopy: imaging of biological membranes in liquid. *Phys. Rev. Lett.* **99,** 046102 (2007).
79. Turner, R. D., Kirkham, J., Devine, D. & Thomson, N. H. Second harmonic atomic force microscopy of living *Staphylococcus aureus* bacteria. *Appl. Phys. Lett.* **94,** 043901 (2009).
80. Raman, A. *et al.* Mapping nanomechanical properties of live cells using multiharmonic atomic force microscopy. *Nature Nanotech.* **6,** 809–813 (2011).
81. Martinez, N. F., Patil, S., Lozano, J. R. & Garcia, R. Enhanced compositional sensitivity in atomic force microscopy by the excitation of the first two flexural modes. *Appl. Phys. Lett.* **89,** 153115 (2006).
82. Patil, S., Martinez, N. F., Lozano, J. R. & Garcia, R. Force microscopy imaging of individual protein molecules with sub-pico Newton force sensitivity. *J. Mol. Recognit.* **20,** 516–523 (2007).
83. Dietz, C. *et al.* Nanotomography with enhanced resolution using bimodal atomic force microscopy. *Appl. Phys. Lett.* **92,** 143107 (2008).
84. Stark, R. W. Dynamics of repulsive dual-frequency atomic force microscopy. *Appl. Phys. Lett.* **94,** 063109 (2009).
85. Albonetti, C., Casalini, S., Borgatti, F., Floreano, L. & Biscarini, F. Morphological and mechanical properties of alkanethiol SAM investigated by bimodal AFM. *Chem. Comm.* **47,** 8823–8825 (2011).
86. Li, W., Cleveland, J. P. & Proksch, R. Bimodal magnetic force microscopy: separation of short and long range forces. *Appl. Phys. Lett.* **94,** 163118 (2009).
87. Stark, R. W., Naujoks, N. & Stemmer, A. Multifrequency electrostatic force microscopy in the repulsive regime. *Nanotechnology* **18,** 065502 (2007).
88. Bostanci, U., Abak, M. K., Aktas, O. & Dâna, A. Nanoscale charging hysteresis measurements by multifrequency electrostatic force spectroscopy. *Appl. Phys. Lett.* **92,** 093108 (2008).

89. Kawai, S. *et al.* Ultrasensitive detection of lateral atomic-scale interactions on graphite (0001) via bimodal dynamic force measurements. *Phys. Rev. B* **81,** 085420 (2010). **This paper reports bimodal excitation and detection of flexural and torsional modes compatible with frequency modulation AFM and ultrahigh-vacuum environments**.
90. Balke, N. *et al.* Nanoscale mapping of ion diffusion in a lithium-ion battery cathode. *Nature Nanotech.* **5,** 749–754 (2010). **The multiparameter acquisition capabilities of the band excitation method are exploited to generate nanoscale maps of lithium-ion migration in batteries**.
91. Balke, N. *et al.* Real space mapping of Li-ion transport in amorphous Si anodes with nanometer resolution. *Nano Lett.* **10,** 3420–3425 (2010).
92. Sahin, O. & Erina, N. High-resolution and large dynamic range nanomechanical mapping in tapping-mode atomic force microscopy. *Nanotechnology* **19,** 445717 (2008).
93. Dong, M., Husale, S. & Sahin, O. Determination of protein structural flexibility by microsecond force spectroscopy. *Nature Nanotech.* **4,** 514–517 (2009).
94. Husale, S., Persson, H. H. J. & Sahin, O. DNA nanomechanics allows direct digital detection of complementary DNA and microRNA targets. *Nature* **462,** 1075–1078 (2009).
95. Dong, M. & Sahin, O. A nanomechanical interface to rapid single-molecule interactions. *Nature Commun.* **2,** 247 (2011).
96. Dokukin, M. E., Guz, N. V., Gaikwad, R. M., Woodworth, C. D. & Sokolov, I. Cell surface as a fractal: normal and cancerous cervical cells demonstrate different fractal behavior of surface adhesion maps at the nanoscale. *Phys. Rev. Lett.* **107,** 028101 (2011).
97. Kolosov, O. & Yamanaka, K. Nonlinear detection of ultrasonic vibrations in an atomic-force microscope. *Jpn. J. Appl. Phys.* **32**, L1095–L1098 (1993).
98. Hu, S., Su, C. & Arnold, W. J. Imaging of subsurface structures using atomic force acoustic microscopy at GHz frequencies. *J. Appl. Phys.* **109,** 084324 (2011).
99. Shekhawat, G. S. & Dravid, V. P. Nanoscale imaging of buried structures via scanning near-field ultrasound holography. *Science* **310,** 89–92 (2005). **First report on nanomechanical holography experiments, providing images of subsurface features in microelectronic devices and cells**.
100. Tetard, L., Passian, A. & Thundat, T. New modes for subsurface atomic force microscopy through nanomechanical coupling. *Nature Nanotech.* **5,** 105–109 (2010).
101. Tetard, L. *et al.* Elastic phase response of silica nanoparticles buried in soft matter. *Appl. Phys. Lett.* **93,** 133113 (2008).
102. Tetard, L. *et al.* Imaging nanoparticles in cells by nanomechanical holography. *Nature Nanotech.* **3,** 501–505 (2008).
103. Shekhawat, G., Srivastava, A., Avashty, S. & Dravid, V. Ultrasound holography for noninvasive imaging of buried defects and interfaces for advanced interconnect architectures. *Appl. Phys. Lett.* **95,** 263101 (2009).
104. Garcia-Sanchez, D., Paulo, A. S., Esplandiu, M. J., Perez-Murano, F. & Bachtold, A. Mechanical detection of carbon nanotube resonator vibrations. *Phys. Rev. Lett.* **99,** 085501 (2007).
105. Garcia-Sanchez, D. *et al.* Imaging mechanical vibrations in suspended graphene sheets. *Nano Lett.* **8,** 1399–1403 (2008).
106. Garcia, R. Images from below the surface. *Nature Nanotech.* **5,** 101–102 (2010).
107. Diebold, A. C. Subsurface imaging with scanning ultrasound holography. *Science* **310,** 61–62 (2005).

Acknowledgements

We are grateful for financial support from the Ministerio de Ciencia e Innovación (CSD2010-00024, MAT2009-08650).

Additional information

The authors declare no competing financial interests. Reprints and permission information is available online at http://www.nature.com/reprints. Correspondence should be addressed to R.G.